# Defense Technical Information Center
## Compilation Part Notice

## ADP012516

TITLE: Crystalline Ion Beams in the RF Quadrupole Storage Ring
PALLAS

DISTRIBUTION: Approved for public release, distribution unlimited

This paper is part of the following report:

TITLE: Non-Neutral Plasma Physics 4. Workshop on Non-Neutral Plasmas
[2001] Held in San Diego, California on 30 July-2 August 2001

To order the complete compilation report, use: ADA404831

The component part is provided here to allow users access to individually authored sections
of proceedings, annals, symposia, etc. However, the component should be considered within
the context of the overall compilation report and not as a stand-alone technical report.

The following component part numbers comprise the compilation report:
ADP012489 thru ADP012577

# Crystalline Ion Beams in the
# RF Quadrupole Storage Ring PALLAS

U. Schramm, T. Schätz, and D. Habs

*Ludwig-Maximilians-Universität München, Sektion Physik, D-85748 Garching, Germany*

**Abstract.**
We report on the crystallization of laser cooled $Mg^+$ ion beams circulating in the table-top rf quadrupole storage ring PALLAS at a velocity of 2800 m/s (beam energy 1 eV). A sudden collapse of the transverse beam size and the low velocity spread clearly indicate the phase transition to a one-dimensional linear string of ions. This crystalline beam shows exceptional stability, surviving for more than 3000 revolutions without cooling. Close to the phase transition, the spatial beam profile of non-crystalline beams was found to exhibit an unexpected two component Gaussian distribution. Although its origin is not yet fully understood, we can exploit this effect for the identification of two- and three-dimensional crystalline beams.

## INTRODUCTION - THE QUEST FOR CRYSTALLINE BEAMS

Threading ions like pearls on a string in high-energy storage rings by freezing out the inter-particle motion [1, 2, 3, 4, 5] opens opportunities far beyond the means of standard accelerator physics [6, 7]. The usual heating due to collisions of particles within the beam almost completely vanishes, giving rise to a state of unprecedented brilliance and exceptional stability. To reach this ultimate goal, beam cooling techniques were improved continuously. With electron cooling, very dilute beams of highly charged ions were observed to exhibit liquid-like order [8, 9] with unique applications in mass spectrometry [10]. With refined laser cooling methods [11, 12], an ambiguous reduction of intra-beam heating [13] was reported for $^9Be^+$ ion beams. Space-charge limited densities were reached for laser cooled $^{24}Mg^+$ ion beams [14], but no clear evidence for beam crystallization has been found in high-energy storage rings so far.

This fact stands in contrast to the routine generation of elongated ion crystals at rest in ring [15] and linear traps [16, 17]. As an illustration and as a reference, in fig. 1 we present images of ion crystals at rest [6, 18], gained with our storage ring PALLAS (PAul Laser cooLing Acceleration System), described below. Ions appear ordered since their mutual Coulomb-repulsion overcomes their mean kinetic energy. The overall Coulomb-repulsion is compensated by an external parabolic trapping potential $\Psi(r,z)$. A strong asymmetry in the radial and longitudinal confinement [18] leads to the prolate shape of the crystals. The formation of the crystalline structure is well understood [3, 15, 17, 19, 20]. The Coulomb-crystal evolves from a linear string of ions over a zig-zag band to three-dimensional helices when the dimensionless linear ion density $\lambda = (N/z) \cdot a$ [19], $N$ denoting the number of particles and $a$ the Wigner-Seitz radius, increases. This can be achieved either by adding more ions, or by reducing the radial confinement.
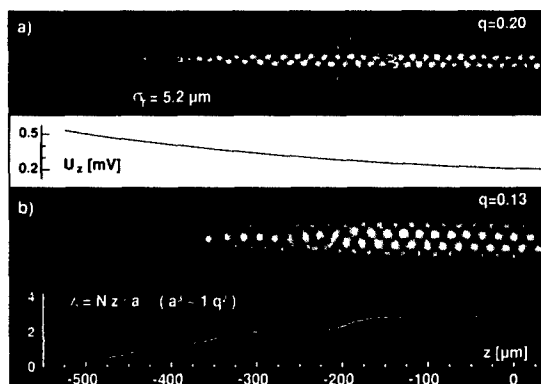
**FIGURE 1.** Fluorescence images of ion crystals at rest in PALLAS. In addition to the radial confinement in the rf quadrupole, the ions are confined longitudinally in a comparably weak static potential $U_z$. The Coulomb-crystal becomes more complex when the linear ion density $\lambda$ increases with lowered confining potential from a) to b) or when it increases step-wise along the axis $z$, as illustrated in b). (Reprinted from [6] with permission from Macmillan Magazines, Ltd.)

In high-energy storage rings, gaseous (emittance dominated) ion beams are heated by intra-beam scattering. In combination with the varying focusing and bending elements, this mechanism couples part of the beam energy into the random ion motion. Cooling now increases the phase space density of the beam, and further amplifies the scattering rate [21, 22]. For a given cooling rate, this vicious circle could only be overcome by increasing the number of focusing sections in the storage ring [23, 24] to achieve a more continuous focusing, or by choosing a sufficiently low ion density [13]. Once having attained the ordered state with sufficient cooling, this heating mechanism should vanish and the beam should collapse to the crystalline state. Additionally, the maintenance of a crystalline beam is expected to impose severe restrictions to the storage ring lattice [23, 25, 20]. The excitation of oscillatory modes of an ion crystal passing through the periodic bending and focusing sections has to be carefully avoided. Numerical simulations yield that to maintain a beam crystal (and, more fundamental, to prevent envelope instabilities of space charge dominated beams [26, 27]), the number of repeating focusing sections $P$ (the periodicity of the ring) has to be larger than $2\sqrt{2} \cdot Q$, the storage ring tune $Q$ being the number of radial oscillations per revolution [28]. This criterion coincides with the validity criterion for treating (time dependent) strong focusing in the (time-averaging) smooth approximation [29]. Also, the beam has to withstand shear in the bending sections which implies that large crystalline beams must orbit with constant angular velocity.

## THE RF QUADRUPOLE STORAGE RING PALLAS

To bridge this gap and to experimentally elucidate the conditions necessary for attaining and maintaining crystalline beams in high-energy rings, we constructed the low-energy

236

rf quadrupole storage ring PALLAS. Sketched in fig. 2, it can be considered as a ring-shaped quadrupole ion guide [15, 29, 30, 18, 6]. The bending radius of the ring amounts to $C/2\pi = 57.5$ mm at an aperture of the quadrupole structure of $r_0 = 2.5$ mm. For radial confinement and bending of the ion beam, a typical rf voltage $U_{rf} = 350$ V at a frequency $\Omega = 2\pi \cdot 6.3$ MHz is applied between the quadrupole ring electrodes. The resulting harmonic pseudo-potential $\Psi(r) = qU_{rf}/8 \cdot (r/r_0)^2$ is characterized by the stability parameter $q = 2eU_{rf}/m\Omega^2 r_0^2 \approx 0.28$, where $e$ and $m$ stand for the charge and mass of the $^{24}$Mg$^+$ ion [31]. The corresponding single-particle secular frequency amounts to $\omega_{sec} = q\Omega/\sqrt{8} = 2\pi \cdot 625$ kHz. This transverse oscillation in the confining pseudo-potential is equivalent to the betatron oscillation [28] of particles in a synchrotron with its alternating focusing and de-focusing magnets. In the quadrupole ring, these discrete but periodic structures are represented by the alternating phase of the rf voltage. The focusing conditions of a beam of velocity $v \approx 2800$ m/s are described by the number of oscillations per round-trip $Q = \omega_{sec}/2\pi \cdot C/v \approx 80$ and the periodicity of the lattice $P = \Omega/2\pi \cdot C/v \approx 800$. Evidently, the postulated maintenance conditions for crystalline beams are fulfilled $(P = \sqrt{8}/q \cdot Q)$. However, the tune and the periodicity can be varied independently to investigate their influence on the stability of crystalline beams.

PALLAS is surrounded by sixteen segmented drift tubes, which can either be used to transport and position ions along the orbit [18] or to manipulate the velocity distribution of stored ion beams [6, 7]. Their voltage penetration at the closed orbit amounts to 0.5 % [30]. Care has been taken to keep potential distortions at the orbit below 100 meV and to provide perfect grounding of the drift tubes to enable circulating ion beams at low velocities. The ions are Doppler-cooled on the closed $3s^2S_{1/2} - 3p^2P_{3/2}$ transition. Two frequency doubled dye lasers provide the required wavelength of 280 nm at an intensity close to saturation. The resonance fluorescence is recorded either with a fast photo-multiplier (PM) or imaged with an intensified CCD camera.
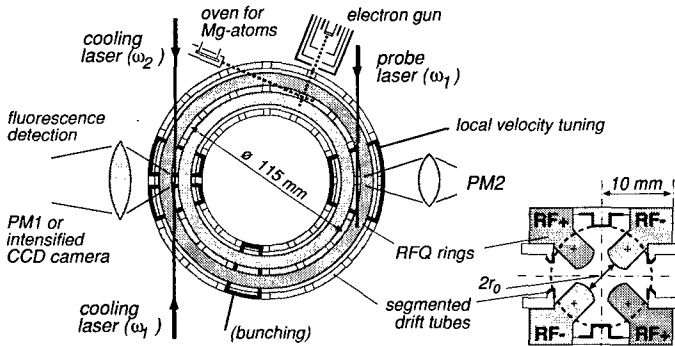


**FIGURE 2.** Axial and radial cut through the rf quadrupole storage ring PALLAS. The circumference of the orbit enclosed by the ring-shaped quadrupole electrodes amounts to $C = 361$ mm. Sixteen segmented drift tubes are distributed around the ring and can be powered individually. The accented tubes are used to localize ions in the laser cooling section, to locally shift the velocity distribution for monitoring purposes, or to bunch an ion beam. To load the ring, a weak beam of $^{24}$Mg-atoms is ionized inside the trapping volume by a focused electron beam and simultaneously laser-cooled to zero velocity.

237

# 1D CRYSTALLINE ION BEAMS (STRINGS)

Ions are accelerated by the light pressure of the continuously tuned co-propagating laser beam (force: $+F_1$). The force profiles are sketched in fig. 3a). The final beam velocity is defined to $v = 2800\,\text{m/s}$ by the counter-propagating and thus decelerating laser ($-F_2$), held at fixed frequency. The longitudinal velocity spread of the beam is reduced by the dispersive character of the combined laser force (optical molasses). The typical behaviour of a cold ion beam is shown in fig. 3a). The fluorescence rate increases, as the detuning of the co-propagating laser is decreased. Then, as it approaches the resonance, the forces start to compensate and the rate drops off again. An increase of the confining potential drastically changes the behaviour, as demonstrated in fig. 3b). Here (grey curve), at first the fluorescence follows the previous curve, then decreases abruptly, and subsequently rises to a sharp peak whose width is dominated by the saturation broadened line-width of the transition. This signature of an abrupt decrease, marked by the arrow, has been previously observed in ion traps [32, 33] and indicates the phase transition to the crystalline state. After a slight reduction of the confining potential, the phase transition cannot be resolved any more (black curve). This suggests that the ions are confined sufficiently strong to form a string but do not experience unnecessary rf heating, which is responsible for the visibility of the above phase transition [6].

For the calibration of the typical fluorescence yield per ion in a crystalline beam, the absolute number of ions in an ion crystals at rest was counted. These ions were accelerated and the corresponding fluorescence rate was measured. A typical peak rate of 3 kHz per ion (in a 1 mm window) subject to the scanning co-propagating laser (as in fig. 3b and fig. 6a) was determined. The absolute fluorescence rate of a non-crystalline beam amounts to about 30% of the crystalline.

The phase transition is furthermore pinpointed by the sudden decrease of the transverse beam size shown in fig. 4. The transition is induced by increasing the radial fo-
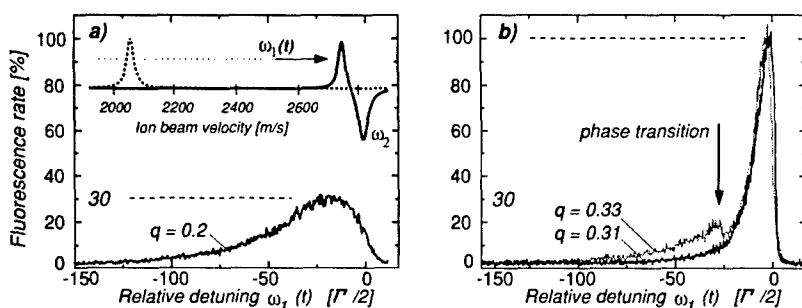


**FIGURE 3.** Fluorescence rate of the ion beam as a function of the frequency detuning of the co-propagating laser (in terms of half the natural transition line width $\Gamma = 2\pi \cdot 42.7\,\text{MHz}$). This accelerating laser is slowly tuned (within 4s) towards the resonance with the counter-propagating, decelerating laser at fixed frequency, which defines the nominal velocity. Fig. a) shows the relative signal of a non-crystalline beam, where in fig. b), the marked discontinuity is characteristic of the phase transition to the crystalline beam. The crystalline beam contained 18,000 Mg$^+$ ions, as deduced from the absolute fluorescence rate.(Reprinted from [6] with permission from Macmillan Magazines, Ltd.)
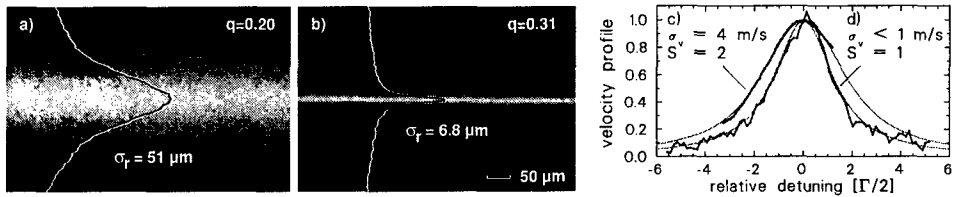
**FIGURE 4.** Transverse beam profiles before a) and after b) the phase transition, which is induced by increasing the confining potential. For a probe of the longitudinal velocity distribution, the local ion velocity is varied periodically (tube voltage amplitude $\approx 60\,\text{mV}$, frequency=1 Hz) inside the pair of drift tubes opposite to the cooling section and thus tuned over the resonance with the fixed frequency probe laser. The corresponding fluorescence rate is recorded. Voigt-profiles (grey lines) are used to disentangle the Doppler-contribution $\sigma_v$ for the two measurements from the saturation ($S$) broadened width of the $3s^2S_{1/2} - 3p^2P_{3/2}$ transition. (Reprinted from [6] with permission from Macmillan Magazines, Ltd.)

cusing strength. Since only the longitudinal ion motion is directly laser cooled, this procedure is necessary to enhance the coupling between the ions and thus the cooling of the transverse ion motion. The spatial profile of the crystalline beam coincides with that of a string of ions at rest (fig. 1a) which is, however, close to the spatial resolution of the imaging system. The number of particles in the string (18,000) denotes a mean inter-particle distance $d \approx 20\,\mu\text{m}$ and thus a linear density $\lambda = 0.4$ which is consistent with the assumption of the formation of a linear string [19]. The beam radius $\sigma_r$ corresponds to an initial transverse temperature of $T_\perp = 30\,\text{K}$ for the non-crystalline and to a resolution limited value of $T_\perp < 0.4\,\text{K}$ for the crystalline beam.

The longitudinal velocity spread of the beam was probed opposite to the cooling section (see fig. 2). Since the probe laser beam was derived from the cooling beam, it could not be frequency tuned. For the detection of a velocity dependent fluorescence signal, the ions were velocity shifted (3% of the beam velocity over a path length of 20 mm) while entering and leaving the pair of drift tubes accented in fig. 2. For a slow (1 Hz) periodic variation of the resulting local ion velocity inside the tube, the fluorescence rate was recorded. To assure that the crystalline structure was not affected, the shape of the beam profile was monitored. The resulting line profiles in fig. 4c) and d) reveal a width of the velocity distribution of 4 m/s ($T_\parallel = 50\,\text{mK}$) for the cold but non-crystalline beam and less than 1 m/s ($T_\parallel < 3\,\text{mK}$) for the crystalline beam, close to the Doppler-limit of 1 mK.

Usually, the inter-ion coupling strength is described by the plasma parameter $\Gamma_p = (e^2/4\pi\varepsilon_0 d) \cdot (1/kT)$, the ratio of the mutual potential energy of ions to their mean thermal energy $kT$. In the longitudinal degree of freedom, $\Gamma_p$ amounts to 250 for the circulating ion string. It even exceeds the theoretical threshold of 180 which is required for the formation of three-dimensional ion crystals [34, 20]. The independent measurement of the transverse temperature of the crystal reveals a value of $\Gamma_p > 2$. This value consistently points towards strong coupling, where both components have to be identical, since, for ion beams, a collapse of the beam heating due to intra-beam scattering is expected for $\Gamma_p > 0.5$ [21, 22]. In summary, the full phase space density has

been determined to increase by a factor of at least $10^4$ and, assuming $T_\perp = T_\parallel$, beyond $10^6$ in the above phase transition [6].

Moreover, already the weakly confined non-crystalline beam (fig. 4a and c) appears to show some Coulomb-order [7]. Its longitudinal temperature leads to a plasma parameter $\Gamma_p > 3$ with the assumption that the typical inter-ion distance is of the order of the radial beam extension $d \sim 2 \cdot \sigma_r$. Under this anisotropic condition ($T_\parallel \ll T_\perp$), the ions perform more than ten betatron oscillations during one binary collision [9]. Therefore, the particles can be regarded as smeared out in the transverse direction by their fast oscillation, but localized in the longitudinal to within the mean particle separation of $\bar{d} \approx 20\,\mu$m. They behave like transverse discs which cannot overtake each other, and Coulomb-order over several neighbouring discs should occur. One expects a partial decoupling of the longitudinal and transverse motion [35], responsible for the inefficient indirect cooling of the transverse motion in the weak confining potential.

# STABILITY OF ION CRYSTALS AND CRYSTALLINE BEAMS

One of the outstanding properties of ion crystals is their elasticity which leads to a strong suppression of the coupling of the periodic rf motion into random thermal motion [36]. Under continuous laser-cooling, circulating ion strings were observed to survive for many hours without any significant ion loss. For the qualitative study of the heating rates, both cooling lasers were simultaneously blocked for a given period of time. The lasers were unblocked and the fluorescence rate was measured [6, 7]. For the ion crystal at rest (a helix as depicted in fig. 1b), the fluorescence rate immediately reappears at its full strength for blocking periods of up to 90 s, as shown in fig. 5a)-c). This indicates the persistence of the crystalline state. In contrast, after a blocking time of
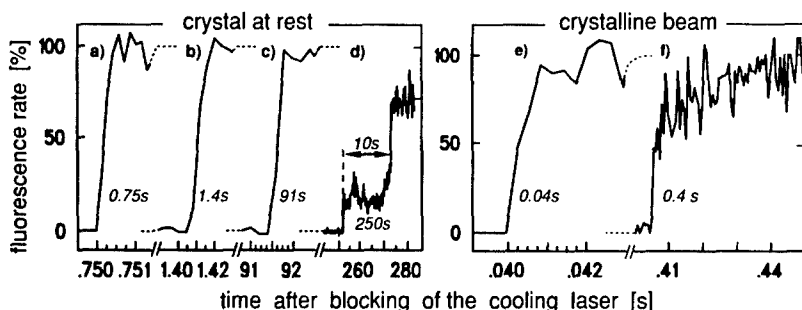


**FIGURE 5.** Fluorescence signal of the ion crystal at rest and the crystalline beam after blocking and unblocking the cooling lasers. The crystal at rest a)-d) survives blocking periods of the order of seconds to minutes, where for a) the time resolution of $250\,\mu$s excludes the possibility of melting and subsequent recrystallization within the rise-time of the fluorescence signal. For the blocking period of 250 s the crystal melts d) and re-crystallizes after 10 s of cooling on a time-scale of seconds. The crystalline beam e)-f) shows an instantaneous recovery after 40 ms e). After blocking the cooling for 400 ms f), the count rate jumps back to 50 % of the initial level and fully recovers within a time scale of 10 ms. (Reprinted from [6] with permission from Macmillan Magazines, Ltd.)

250 s (fig. 5d), the fluorescence reappears to a level of only 25 % which is characteristic for the gaseous cloud (compare fig. 3a and b). After the melting of the crystal, the ions are heated due to Coulomb-scattering in the presence of the rf field. Ions are lost out of the velocity range defined by the relative detuning of the two cooling lasers. This results in a strong reduction of the cooling rate, as reflected in the comparably long time span of 10 s needed for the re-crystallization. The survival time of $6 \cdot 10^8$ rf periods reasonably coincides with recent simulations [36] of ion crystal stability in time-varying potentials. A similar procedure for the crystalline ion beam also results in an immediate restoration of the fluorescence signal after 40 ms of blocking the lasers (fig. 5e). After a period of 400 ms (fig. 5f) the signal reappears at a level of 50 %, a signal rate that reflects the survival of a less dense crystalline beam. Subsequently, the signal fully recovers on a ms time scale. We therefore propose the formation of a two phase regime, in which a string of decreased ion number survives. From the fast recovery time and the fact that the beam is only cooled on a fraction of 1 % of the orbit, it seems unlikely that ions are dominantly heated in longitudinal direction. Probably, a fraction of the beam either forms a cold halo or starts to show the disc-like behaviour, discussed above.

## 2D-3D CRYSTALLINE BEAMS (ZIG-ZAGS AND HELICES)

The attainment of crystalline beams of higher linear density ($\lambda > 0.7$) then the strings discussed so far is of general interest concerning the feasibility of increased luminosity at high-energy rings. In particular, the question of shear and the consequence of cooling to constant angular velocity becomes important as well as the increased coupling of the beam to the time-varying confining potential [23, 25, 4, 5, 20]. However, the unambiguous identification of 2D and 3D crystalline beams becomes more difficult.

In fig. 6a)-b), we present images of a crystalline beam right at the threshold of the transition from the 1D string to the 2D zig-zag configuration. A slight decrease of the confining potential ($q = 0.22 \rightarrow 0.20$) corresponds to an increase in the linear density of $\lambda = 0.70 \rightarrow 0.77$ and therefore to the evolution of a zig-zag beam [19]. In fig. 6c) the latter profile b) is enlarged. Its absolute shape can be reproduced by the sum of two profiles of the corresponding linear string (fig. 6a), divided in amplitude by a factor of two and displaced vertically by $\pm 6\mu$m. Furthermore, we observed (fig. 6d) a similar discontinuity in the fluorescence signal when the laser is tuned as in the case of the string (fig. 3b), which supports the interpretation of the beam profile. The orientation of the zig-zag beam is always vertical to circumvent shear [7]. Compared to the profile of 2D crystals at rest (fig. 1a), the contrast of the beam profile is markedly reduced, which still could be a problem of the comparably low overall count-rate.

For the description of the measured profiles of the crystalline and of the non-crystalline beams (see fig. 4 and 6) close to the phase transition, a double Gaussian distribution with the width $\sigma^c$ and $\sigma^h$ and the amplitude $I^c$ and $I^h$ of a core and a halo component has to be applied. In fig. 7, the amplitude ratio $I^h/I^c$ as well as the width of the halo $\sigma^h$ are shown as a function of the width $\sigma^c$ of the central core. For the non-crystalline beams (open symbols), where the width is a measure of the temperature, $\sigma^c$ and $\sigma^h$ are normalized to $U_{rf} = 350 \, \text{V}$ ($q = 0.28$) according to $kT \propto \Psi(\sigma) \propto (U_{rf} \cdot \sigma)^2$.
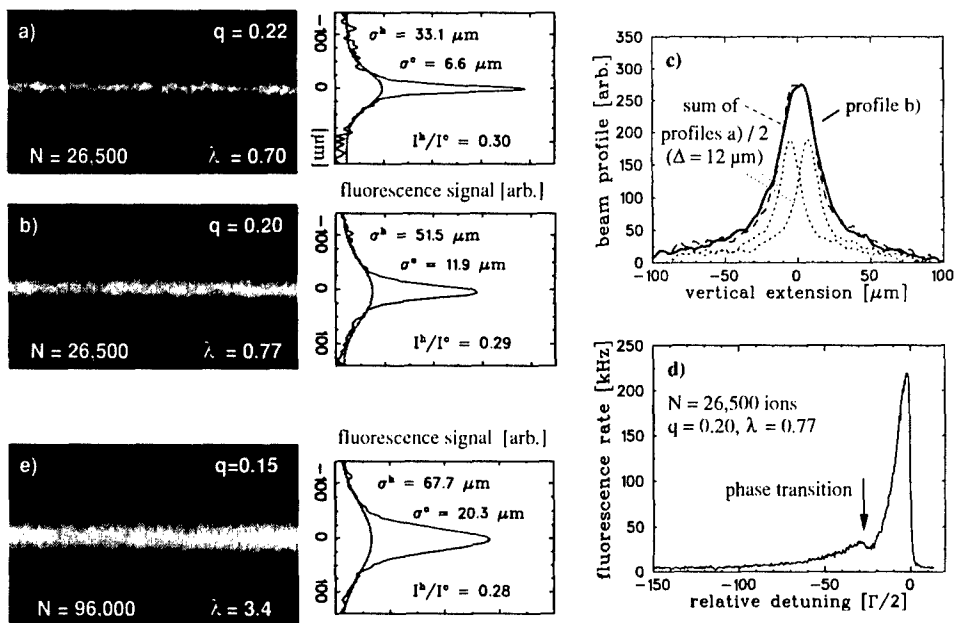
**FIGURE 6.** Vertical beam profiles of the same beam for two slightly different confining potentials a)-b), which demonstrate the transition from the string to the zig-zag. In c), the shape of this zig-zag beam is analyzed, where in d), its fluorescence rate is depicted as a function of the (dynamic) laser detuning. The profile e) belongs to a 3D crystalline beam, presumably a helix with a string in the center.

For the transition to the 1D crystalline beam around $\sigma^c \approx 10\,\mu m$, we find a significant reduction of the amplitude ratio of the halo to the core component $I^h/I^c$. This separation is even more pronounced in the original data (some non-crystalline data points were recorded at low rf voltages of about $U_{rf} \approx 150 - 250\,V$ and thus plotted at radii $\sigma^c$, normalized to lower values). The remaining halo contribution is observed to coincide for all crystalline ion strings in flight and at rest, recorded in PALLAS and taken from ref. [15]. The coincidence suggests that this contribution might be due to scattering of light in the optical imaging system or at least due to a process not attributed to the crystalline beam. Furthermore, the amplitude ratio remains nearly constant for the zig-zag beam (marked with the left arrow) although the width of its core component has naturally increased. This fact is valid also for larger crystals at rest, where the width of the core can be described by a Woods-Saxon profile. This set of reference data allows the distinction of 1D and 2D crystalline beams from non-crystalline beams although the reason for the significant halo component observed in the transverse profiles of the non-crystalline beams remains unclear at the moment.

The beam profile, presented in fig. 6e), belongs to a beam of 96,000 ions. Already from the comparably small width in relation to the high particle number, one can roughly estimate the beam to be crystalline (compare fig. 4a). The ratio $I^h/I^c$ (marked with the right arrow in fig. 7) clearly corresponds to that of a crystalline structure. The linear
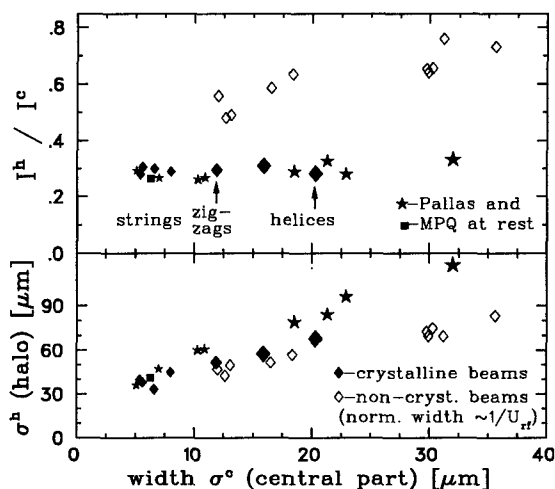
**FIGURE 7.** For coasting beams as well as for a variety of ion crystals at rest, the behaviour of the beam profile, described by a two component Gaussian distribution, is shown as a function of the width $\sigma^c$ of the central component. For the non-crystalline beams (open symbols), $\sigma^c$ and $\sigma^h$ are normalized to $U_{rf} = 350\,\text{V}$. The marked points correspond to the beam profiles presented in the previous figure.

density of $\lambda = 3.4$ corresponds to a helix encircling a string [19]. Though cooled to constant linear velocity, this large crystalline beam withstands bending shear. According to [23], for the high betatron tune of $Q \approx 40 > \lambda$, the Coulomb force within the crystal is strong enough to arrange constant angular velocity.

Concerning the formation of the two component profiles which were observed to be characteristic for the non-crystalline beams in PALLAS, we can only speculate at present [7]. The linear relation of $\sigma^h$ and $\sigma^c$ suggests some correlation between both components. Since the scaling is independent of the longitudinal cooling strength and of the focusing potential, a radius dependent heating rate seems to be less probable. The width $\sigma$ of a beam is related to its transverse temperature $kT_\perp \propto m\omega_{sec}^2 \sigma^2$. Thus, one could imagine the co-existence of individual (halo) ions and short string fragments (core) of different collective mass at the same temperature $T_\perp$ to describe the two components. Both phases could simultaneously exist at different orbital positions in the storage ring, since cooling is restricted to only a fraction of the circumference. In ion trap experiments [32], bi-stability is well established. Also transverse oscillations of short crystalline strings were observed [18]. However, the effect has to be further explored.

## SUMMARY AND OUTLOOK

The realization of circulating ion strings [6] and of first vertical zig-zag and helical structures in PALLAS allows to experimentally investigate many questions concerning the formation of crystalline beams in high-energy rings, known up to now only from simulations [4, 5, 20]. The focusing conditions, the linear ion density, and the beam

243

velocity can be independently varied, the latter presently between $10^3$ and $10^4$ m/s. In the near future, we plan to implement optical Schottky-diagnosis to study noise spectra of cold and crystalline beams, which carry further information about collective effects. Furthermore, bunching of an ion beam was studied and will be reported elsewhere [7].

# ACKNOWLEDGEMENTS

# REFERENCES

1.   Parkhomchuk, V., "Review of Electron Cooling Investigation at the Novosibirsk INP", in [5], pp. 409-420 and Pestrikov, D.V., "Schottky Spectra and Crystalline Beams", in *ibid.*, pp. 275-294.
2.   Schiffer, J.P., Kienle, P., *Z. Phys.* **A321**, 181 (1985).
3.   Rahman, A., Schiffer, J.P., *Phys. Rev. Lett.* **57**, 1133-1136 (1986).
4.   Hasse, R.W., Hofmann, I., Liesen, D., (eds.), *Crystalline Ion Beams*, GSI report, GSI-89-10, (1989).
5.   Maletic, D.M., Ruggiero, A.G., (eds.), *Crystalline Beams*, World Scientific, Singapore, 1996.
6.   Schätz, T., Schramm, U., Habs, D., Nature (London), in press (16/8/2001).
7.   Schramm, U., Schätz, T., Habs, D., submitted to *Phys. Rev. Lett.* (2001).
8.   Steck, M., et al., *Phys. Rev. Lett.* **77**, 3803-3806 (1996).
9.   Hasse, R.W., *Phys. Rev. Lett.* **83**, 3430-3433 (1999) and these proceedings.
10.  Radon, T., et al., *Nucl. Phys.* **A 677**, 75-99 (2000).
11.  Lauer, I., et al., *Phys. Rev. Lett.* **81**, 2052-2055 (1998).
12.  Eisenbarth, U., et al., Nucl. Instr. and Meth. **A 441**, 209-218 (2000).
13.  Eisenbarth, U., et al., *Hyp. Int.* **127**, 223-235 (2000) and these proceedings.
14.  Madsen, N., et al., *Phys. Rev. Lett.* **83**, 4301-4304 (1999).
15.  Birkl, G., Kassner, S., Walther. H., *Nature* **357**, 310-313 (1992).
16.  Raizen, M.G., et al., *Phys. Rev. A* **45**, 6493-6501 (1992).
17.  Drewsen, M., et al., *Phys. Rev. Lett.* **81**, 2878-2881 (1998) and these proceedings.
18.  Schramm, U., Schätz, T., Habs, D., "Laser-cooling of Ions and Ion Acceleration in PALLAS", in *Appl. of Acc. in Research and Industry*, edt. J.L. Duggan, AIP Conf. Proc. **576**, in press (2001).
19.  Hasse, R.W., Schiffer, J.P., *Annals of Phys.* **203**, 419-448 (1990).
20.  Habs, D., Grimm, R., *Ann. Rev. Nucl. Part. Sci.* **45**, 391-428 (1995).
21.  Seurer, M., Spreiter, Q., Toepffer, C., "IBS in Dense and Cold Beams", in [5], pp. 311-328.
22.  Wei, J., et al., "Diverse Topics in Crystalline Beams", in [5], pp. 229-252.
23.  Schiffer, J.P., "The Physics of Crystalline Ion Beams", in [5], pp. 217-228.
24.  Spreiter, Q., Seurer, M., Toepffer, C., *Nucl. Instr. Meth.* **A 364**, 239-242 (1995).
25.  Wei, J., Okamoto, H., Sessler, A.M., *Phys. Rev. Lett.* **80**, 2606-2609 (1998).
26.  Riabko, A., et al., *Phys. Rev.* **E 51**, 3529-3546 (1995).
27.  Kjaergaard, N., Drewsen, M., *Phys. of Plasmas* **8**, 1371-1375 (2001).
28.  Bryant, P.J., Johnson, K., *Circular Accelerators and Storage Rings*, Cambridge Univ. Press, 1993.
29.  Schätz, T., et al., "Towards crystalline ion beams - the PALLAS ring trap", in *Trapped Charged Particles and Fund. Phys.*, eds. D. Dubin, D. Schneider, AIP Conf. Proc. **457**, 1999, pp. 269-273.
30.  Schätz, T., Schramm, U., Habs, D., Hyp. Int. **115**, 29-36 (1998).
31.  P.K. Gosh, *Ion Traps*, Clarendon Press, Oxford (1995).
32.  Diedrich, F., et al., Phys. Rev. Lett. **59**, 2931-2934 (1987).
33.  Blümel, R., et al., *Nature* **334**, 309-313 (1988).
34.  Dubin, D.H.E., *Phys. Rev. A* **42**, 4972-4982 (1990).
35.  Hasse, R.W., Phys. Rev. A **46**, 5189 (1992).
36.  Schiffer, J.P., et al., *Proc. Natl. Acad. Sci. USA* **97**, 10697-10700 (2000)